The internal-strain tensor of crystals for nuclear-relaxed elastic and piezoelectric constants: On the full exploitation of its symmetry features

Journal Name

ARTICLE TYPE

Cite this: DOI: 10.1039/xxxxxxxxxx

Internal-Strain Tensor of Crystals for Nuclear-relaxed Elastic and Piezoelectric Constants: On the Full Exploitation of its Symmetry Features

Alessandro Erba,[a,*]

Received Date
Accepted Date

DOI: 10.1039/xxxxxxxxxx

www.rsc.org/journalname

Symmetry features of the internal-strain tensor of crystals (whose components are mixed second-energy derivatives with respect to atomic displacements and lattice strains) are formally presented, which originate from translational-invariance, atomic equivalences, and atomic invariances. A general computational scheme is devised, and implemented into the public CRYSTAL program, for the quantum-mechanical evaluation of the internal-strain tensor of crystals belonging to any space-group, which takes full-advantage of the exploitation of these symmetry-features. The gain in computing time due to the full symmetry exploitation is documented to be rather significant not just for high-symmetry crystalline systems such as cubic, hexagonal or trigonal, but also for low-symmetry ones such as monoclinic and orthorhombic. Use of the internal-strain tensor is made for the evaluation of the nuclear relaxation term of the fourth-rank elastic and third-rank piezoelectric tensors of crystals, where, apart from a reduction of computing time, the exploitation of symmetry is documented to remarkably increase the numerical precision of computed coefficients.

1 Introduction

The density functional theory (DFT) offers an effective way for the quantum-mechanical calculation of many strain-related tensorial properties of solids, such as the third-rank direct piezoelectric tensor, the fourth-rank elastic tensor, and the fourth-rank photo-elastic (or elasto-optic) tensor.[1–12] By manipulating and combining these fundamental quantities, other tensorial properties can be derived such as elastic compliances, converse piezoelectric coefficients and piezo-optic coefficients. The elements of all of these tensors can be interpreted as total energy derivatives with respect to three kinds of perturbations: periodicity-preserving atomic displacements, homogeneous strains and homogeneous electric fields. A formal account has been reported of the systematic treatment of these three perturbations, when combined together up to second- and third-order.[13,14]

The integrated quantum-mechanical evaluation of all of these tensor components might obviously become a rather computationally prohibitive task, unless particular care is taken in devising efficient algorithms. In this respect, a cleaver exploitation of the usually rich point-symmetry features of crystalline materials can lead to a significant reduction of the number of symmetry-irreducible tensor components to be actually determined, with the corresponding widening of the applicability domain of *ab initio* methods as regards the size of the systems to be investigated. For instance, point-symmetry is known to constrain many components of the piezoelectric, elastic and photo-elastic tensors to be zero or to be equivalent to each other.[15]

Strain-induced response properties of solids can be formally decomposed into a purely electronic "clamped-nuclei" term and a nuclear-relaxation term due to the rearrangement of atomic positions upon strain. The evaluation of the latter is generally much more computationally expensive than that of the former and can be achieved following two alternative approaches: i) performing numerical geometry optimizations to relax atomic positions at actual strained lattice configurations,[16,17] or ii) evaluating in a more analytical fashion the internal-strain tensor of energy second-derivatives with respect to atomic displacements and lattice deformations, as combined with the interatomic force constant Hessian matrix.[13] On the one hand, the former approach allows for an easier exploitation of symmetry given that many solid-state quantum-mechanical packages do perform symmetry-constrained geometry optimizations; on the other hand, though, it is a rather slowly-converging numerical procedure requiring particularly tight convergence criteria to be adopted. As a conse-

[a] *Dipartimento di Chimica, Università di Torino, via Giuria 5, IT-10125 Torino, Italy.*
[*] *E-mail: alessandro.erba@unito.it*

quence, the latter approach is to be preferred as it ensures higher accuracy and requires less severe computational parameters to be used.[18]

This paper aims at formally illustrating the specific symmetry features of the internal-strain tensor, and at devising a computational scheme for their effective exploitation in the quantum-mechanical calculation of nuclear-relaxed strain-induced properties of crystals. The current approach represents an extension to internal-strain components of the strategy originally proposed by Stanton for point-symmetry exploitation in the construction of interatomic force constants of molecules,[19] as generalized to solids.[20] Such a scheme has been implemented into a developmental version of the public CRYSTAL14 program for *ab initio* solid state simulations, which is particularly suitable for exploiting symmetry features of crystals.[20–25]

The structure of the paper is as follows: definitions of both the force-response and displacement-response versions of the internal-strain tensor are given in Section 2.1; expressions for the nuclear-relaxation contribution of both elastic and piezoelectric constants in terms of the internal-strain tensor are given in Section 2.2, where a partition of such term into normal-mode contributions is also introduced; symmetry features of atomic and lattice parameter energy gradients are recalled in Section 2.3; Section 2.4 is devoted to the presentation of the symmetry features of the internal-strain tensor, which originate from translational-invariance, atomic equivalences, and atomic invariances; the technical and computational aspects of the current implementation are discussed in Section 3; results on the symmetry-exploitation are presented and discussed in Section 4 as regards both the gain in computing time and the increased accuracy of computed elastic and piezoelectric constants; conclusions are drawn in Section 5

2 Formalism

2.1 Preliminary Definitions

We consider a crystal belonging to a given space group $\mathscr{G}$ in a reference state in which the three fundamental direct lattice vectors are $\mathbf{a}_1$, $\mathbf{a}_2$ and $\mathbf{a}_3$ so that the corresponding cell volume is $V_0 = \mathbf{a}_1 \cdot (\mathbf{a}_2 \times \mathbf{a}_3)$. In the equilibrium configuration of the crystal, the N atoms within the reference cell (to be labeled with $a, b = 1, \ldots, N$ in the following) are centered at positions $\mathbf{r}_a$.

In order to define the internal-strain tensor Λ, two kinds of perturbations have to be explicitly considered: periodicity-preserving atomic displacements $\mathbf{u}_a$ from equilibrium atomic positions $\mathbf{r}_a$, and lattice deformations. The elements of the force-response internal-strain tensor can be expressed as second-energy derivatives with respect to an atomic displacement and to a lattice distortion:

$$\Lambda_{ai,\alpha j} = \left. \frac{\partial^2 E}{\partial u_{ai} \partial a_{\alpha j}} \right|_{\mathscr{E}} , \tag{1}$$

where u_{ai} are Cartesian components of the displacement vector $\mathbf{u}_a$ of atom a (i=x,y,z), $a_{\alpha j}$ are Cartesian components of lattice vector $\mathbf{a}_\alpha$ (α=1,2,3; j=x,y,z), and the derivative is taken at constant external electric field $\mathscr{E}$ to ensure compatibility with the definition of piezoelectricity to be introduced below. In this basis of atomic Cartesian coordinates and Cartesian lattice vector components, Λ can be given a $3N \times 9$ matrix representation. Let us introduce the symmetric second-rank pure strain tensor η, whose action on an undeformed lattice vector $\mathbf{a}_\alpha$ to get its deformed counterpart $\mathbf{a}'_\alpha$ is given by:

$$a'_{\alpha j} = \sum_k (\delta_{jk} + \eta_{jk}) a_{\alpha k} , \tag{2}$$

where k is a Cartesian index and δ_{jk} is the Kronecker delta. By exploiting relation (2), the elements of the internal-strain tensor in (1) can be transformed from the basis of Cartesian lattice vector components to the one of strain tensor components as follows:

$$\Lambda_{ai,jk} = \left. \frac{\partial^2 E}{\partial u_{ai} \partial \eta_{jk}} \right|_{\mathscr{E}} = \sum_\alpha a_{\alpha k} \left. \frac{\partial^2 E}{\partial u_{ai} \partial a_{\alpha j}} \right|_{\mathscr{E}} . \tag{3}$$

As the pure strain tensor η is symmetric, there are just six independent components η_{jk} to be considered. It is convenient to adopt Voigt's notation, which maps the two Cartesian index notation (jk) into a one index notation (v), where $v = 1 \equiv xx$, $v = 2 \equiv yy$, $v = 3 \equiv zz$, $v = 4 \equiv yz$, $v = 5 \equiv xz$, and $v = 6 \equiv xy$.[15] Accordingly, the internal-strain tensor can be given a $3N \times 6$ matrix representation:

$$\Lambda_{ai,v} = \left. \frac{\partial^2 E}{\partial u_{ai} \partial \eta_v} \right|_{\mathscr{E}} . \tag{4}$$

Let us note that the definition given in Eq. (4) refers to the force-response internal strain tensor, to be distinguished from the displacement-response internal-strain tensor Γ, which describes first-order atomic displacements as induced by a first-order strain:[13]

$$\Gamma_{ai,v} = - \left. \frac{\partial u_{ai}}{\partial \eta_v} \right|_{\mathscr{E}} = \sum_{bj} (H^{-1})_{ai,bj} \Lambda_{bj,v} , \tag{5}$$

where $\mathbf{H}$ is the interatomic force-constant Hessian matrix of energy second derivatives with respect to pairs of periodicity-preserving atomic displacements:

$$H_{ai,bj} = \left. \frac{\partial^2 E}{\partial u_{ai} \partial u_{bj}} \right|_{\mathscr{E},\eta} . \tag{6}$$

When mass-weighted and diagonalized, the force-constant matrix of Eq. (6) provides the vibration frequencies of Brillouin zone-center phonon modes (see below). Some care must be taken in evaluating Eq. (5) in that the force-constant matrix (6) is singular by construction (i.e. it has three null eigenvalues corresponding to the three translational degrees of freedom) and thus can not be inverted as such. The $\mathbf{H}^{-1}$ matrix in Eq. (5) has to be considered a "pseudoinverse" of $\mathbf{H}$ where translational degrees of freedom are projected out, as discussed in detail elsewhere.[13]

2.2 Nuclear Relaxation Contribution of Elastic and Piezoelectric Tensors

It has been shown by a systematic treatment of the simultaneous effect of three kinds of perturbations (atomic displacements, strains and electric fields) on the energy of the system up to second-order, that the internal-strain tensor Λ (or Γ) enters the definition of the nuclear-relaxation contribution (complementary

to the purely electronic, clamped-nuclei one) of elastic constants and piezoelectric coefficients.[13] The elastic constants of a crystal can indeed be expressed as:

$$C_{vw} = \frac{1}{V_0}\frac{\partial^2 E}{\partial\eta_v\partial\eta_w}\bigg|_{\mathscr{E}} = \tag{7}$$

$$= \frac{1}{V_0}\frac{\partial^2 E}{\partial\eta_v\partial\eta_w}\bigg|_{\mathscr{E},u} - \frac{1}{V_0}\sum_{ai}\Lambda_{ai,v}\Gamma_{ai,w}\,, \tag{8}$$

where w is a Voigt's index as v. The first and second terms on the rhs of Eq. (8) represent the electronic clamped-nuclei elastic constants, where atomic positions are not allowed to relax following the strain, and the nuclear relaxation contribution, respectively. Analogously, piezoelectric coefficients can be expressed as the sum of an electronic clamped-nuclei and a nuclear relaxation contribution as follows:

$$e_{kv} = \frac{1}{V_0}\frac{\partial^2 E}{\partial\mathscr{E}_k\partial\eta_v} = \tag{9}$$

$$= \frac{1}{V_0}\frac{\partial^2 E}{\partial\mathscr{E}_k\partial\eta_v}\bigg|_{u} - \frac{1}{V_0}\sum_{ai}Z^*_{k,ai}\Gamma_{ai,v}\,. \tag{10}$$

Here, we do not enter into details about the subtleties related to the distinction between "proper" and "improper" piezoelectric coefficients, which have been extensively discussed elsewhere.[2,13,26–29] The $\mathbf{Z}^*$ tensor in Eq. (10) contains the Born dynamical effective charges:

$$Z^*_{k,ai} = \frac{\partial^2 E}{\partial\mathscr{E}_k\partial u_{ai}}\bigg|_{\eta}\,. \tag{11}$$

2.2.1 Normal-mode Partition

The Γ internal-strain tensor, which enters the definition of the nuclear relaxation contributions of both elastic and piezoelectric constants, is defined in terms of the interatomic force-constant matrix $\mathbf{H}$ in Eq. (5). As anticipated above, if $\mathbf{H}$ is mass-weighted and diagonalized, Brillouin zone-center phonon modes and corresponding vibration frequencies can be determined:

$$\tilde{H}_{ai,bj} = \frac{H_{ai,bj}}{\sqrt{M_a M_b}} \quad \text{and} \quad \tilde{\mathbf{H}}\mathbf{U} = \Xi\mathbf{U}\,, \tag{12}$$

where M_a is the mass of atom a, Ξ is a $3N\times 3N$ diagonal matrix whose eigenvalues $\xi_p = \omega_p^2$ are the squared vibration frequencies (being $p = 1,\ldots,3N$ a phonon mode label) and $\mathbf{U}$ is the $3N\times 3N$ transformation matrix from atomic Cartesian coordinates to corresponding phonon normal mode coordinates. The diagonalization of the mass-weighted interatomic force-constant matrix in Eq. (12) opens the way for a physically meaningful partition of the nuclear relaxation contributions given in Eqs. (8) and (10) in terms of phonon normal modes:

$$C^{\rm nuc}_{vw} = -\frac{1}{V_0}{\sum_p}'\frac{\tilde{\Lambda}_{pv}\tilde{\Lambda}_{pw}}{\omega_p^2}\,; \tag{13}$$

$$e^{\rm nuc}_{kv} = -\frac{1}{V_0}{\sum_p}'\tilde{Z}^*_{k,p}\frac{\tilde{\Lambda}_{p,v}}{\omega_p^2}\,, \tag{14}$$

where $\tilde{\Lambda}$ is the mass-weighted internal-strain tensor ($\tilde{\Lambda}_{ai,v} = \Lambda_{ai,v}/\sqrt{M_a}$) and $\tilde{\mathbf{Z}}^*$ the mass-weighted Born effective charge tensor ($\tilde{Z}^*_{k,ai} = Z^*_{k,ai}/\sqrt{M_a}$) expressed in the basis of the normal modes. Summations are primed in Eqs. (13) and (14) because the three vanishing eigenvalues ω_p^2 are excluded, which correspond to the three translational degrees of freedom.

2.3 Symmetry Features of Atomic and Cell Energy Gradients

The general symmetry operator of a space group $\mathscr{G}$ can be represented by the following symbol:

$$\hat{V}_{R_o,\mathbf{t}} = \{\hat{R}_o|\mathbf{l}_{R_o}+\mathbf{t}\}\,, \tag{15}$$

where $\hat{R}_o$ denotes a proper or improper rotation, $\mathbf{l}_{R_o}$ a fractionary translation, and $\mathbf{t}$ a direct lattice vector. The set of rotations $\hat{R}_o$ constitutes a group (the point-symmetry group $\mathscr{P}$ of the crystal) of order $|\mathscr{P}|$ (with $o = 1,\ldots,|\mathscr{P}|$). We shall use the symbol

$$\hat{V}_{R_o} \equiv \hat{V}_{R_o,\mathbf{0}} = \{\hat{R}_o|\mathbf{l}_{R_o}\}\,, \tag{16}$$

to represent the $|\mathscr{P}|$ translationally non-equivalent symmetry operators of the crystal. For symmorphic space groups all $\mathbf{l}_{R_o}$ are null. We shall start by discussing how atomic energy gradients $f_{ai} = \partial E/\partial u_{ai}$ ($\mathbf{f}_a$ is the atomic gradient vector) and lattice vector energy gradients $g_{\alpha j} = \partial E/\partial a_{\alpha j}$ ($\mathbf{g}_\alpha$ is the lattice vector gradient vector) are transformed by application of point-symmetry operators. In Section 2.4, we will then combine these symmetry-transformation properties to discuss those occurring among internal-strain tensor components, which can be written in terms of f_{ai} and $g_{\alpha j}$ as follows:

$$\Lambda_{ai,\alpha j} = \frac{\partial g_{\alpha j}}{\partial u_{ai}}\bigg|_{\mathscr{E}} \equiv \frac{\partial f_{ai}}{\partial a_{\alpha j}}\bigg|_{\mathscr{E}}\,. \tag{17}$$

2.3.1 Atomic Equivalences

Each symmetry-irreducible atom a_1 in the crystal reference cell (note that in this subsection atomic labels get a subscript to explicitly trace atomic equivalences) is located at an equilibrium position $\mathbf{r}_{a_1}$, which is characterized by a certain site-symmetry identified by a specific point-symmetry sub-group $\mathscr{H}_{a_1}$ defined as the set of those symmetry operators that do not move atom a_1:

$$\mathscr{H}_{a_1} = \{\hat{R}_q\}_{q=1,\ldots,|\mathscr{H}_{a_1}|} \quad \text{where} \quad \hat{R}_q\mathbf{r}_{a_1} = \mathbf{r}_{a_1} \quad \forall\hat{R}_q\in\mathscr{H}_{a_1}\,.$$

Atom a_1 will have $n^{\rm star}_{a_1} - 1$ equivalent atoms generated by application of those symmetry operators which do not belong to $\mathscr{H}_{a_1}$, where $n^{\rm star}_{a_1} = |\mathscr{P}|/|\mathscr{H}_{a_1}|$ is the ratio between the order of the point-symmetry group and the order of the site-symmetry subgroup. Symmetry-equivalent atoms are said to constitute a *star* of atoms. A compact list of those symmetry operators that, once applied to a symmetry-irreducible atom a_1, generate its equivalent atoms in the *star* can be obtained by performing a so-called left-coset partition of $\mathscr{P}$ in terms of $\mathscr{H}_{a_1}$:

$$\mathscr{P} = \sum_{s=1}^{n^{\rm star}_{a_1}}\hat{R}_s\mathscr{H}_{a_1}\,, \tag{18}$$

where the $\hat{R}_s$ are the left-coset representative operators (by convention being $\hat{R}_1 \equiv E$, the identity operator) that, when applied to a_1, provide the corresponding equivalent atoms a_s. The invariant sub-groups $\mathscr{H}_{a_s}$ of the equivalent atoms can then be derived from the reference one as: $\mathscr{H}_{a_s} = \hat{R}_s \mathscr{H}_{a_1} \hat{R}_s^{-1}$. These atomic symmetry equivalences can be exploited to reduce the number of atomic energy gradients $\mathbf{f}_a$ to be computed down to one per *star* of equivalent atoms as the following transformation property applies:

$$\mathbf{f}_{a_s} = \hat{R}_s \mathbf{f}_{a_1} \quad \text{if} \quad \mathbf{r}_{a_s} = \hat{R}_s \mathbf{r}_{a_1} \,. \tag{19}$$

2.3.2 Transformation Properties of Cell Gradients

Upon application of any point-symmetry operator $\hat{R}_o$, cell gradient vectors $\mathbf{g}_\alpha$ transform as fundamental reciprocal lattice vectors $\mathbf{b}_\alpha$ do. For this reason, we shall now briefly discuss symmetry-transformation properties of reciprocal lattice vectors. Given the three fundamental direct lattice vectors $\mathbf{a}_1$, $\mathbf{a}_2$ and $\mathbf{a}_3$ (from now on we shall assume these vectors to refer to the conventional cell for ease of exemplification), the corresponding three reciprocal lattice vectors $\mathbf{b}_1$, $\mathbf{b}_2$ and $\mathbf{b}_3$ are defined through the following orthogonality relation:

$$\mathbf{a}_\alpha \cdot \mathbf{b}_\beta = 2\pi\delta_{\alpha\beta} \quad \text{with} \quad \alpha,\beta = 1,2,3 \,. \tag{20}$$

Whenever a symmetry operator $\hat{R}_o$ is applied to a fundamental reciprocal lattice vector, it is rotated into a linear combination of the three fundamental vectors as:

$$\hat{R}_o \mathbf{b}_\alpha = \sum_\beta c^o_{\alpha\beta} \mathbf{b}_\beta \,, \tag{21}$$

where the coefficients $c^o_{\alpha\beta}$ can be either ± 1 or 0. Correspondingly, as anticipated before, lattice vector energy gradients $\mathbf{g}_\alpha$ transform as:

$$\hat{R}_o \mathbf{g}_\alpha = \sum_\beta c^o_{\alpha\beta} \mathbf{g}_\beta \,, \tag{22}$$

where coefficients $c^o_{\alpha\beta}$ in Eq. (22) coincide with those in Eq. (21). For most Bravais lattices (such as cubic, tetragonal, orthorhombic, monoclinic, triclinic ones), only one coefficient of the linear combinations in Eqs. (21) and (22) is non-null for any given pair o,α. However, for hexagonal and trigonal lattices, two coefficients can be simultaneously different from zero for some pairs o,α.

2.4 Symmetry Features of the Internal-Strain Tensor

The force-response internal-strain tensor Λ defined in Eq. (1) exhibits three main symmetry features: 1) translational invariance, 2) atomic equivalences, and 3) atomic invariances. While property 1) is relatively trivial, properties 3) and 2) require a rigorous symmetry analysis in order to be fully-exploited and are based on the partition of point-group $\mathscr{P}$ given in Eq. (18) in terms of the invariant site-symmetry sub-group proper of each atom and of the corresponding left-coset representatives, which generate the equivalent atoms, respectively.

2.4.1 Translational Invariance (TI)

The energy E of the crystal is invariant with respect to a rigid translation of all atoms by the same displacement along any of the three Cartesian directions, which leads to the following sum-rule for atomic gradients:

$$\sum_a \frac{\partial E}{\partial u_{ai}} = 0 \quad \text{for each} \quad i = x,y,z \,. \tag{23}$$

Condition (23) on the atomic energy gradients, propagates to the internal-strain tensor so that, for each Cartesian component $a_{\alpha j}$ of a fundamental direct lattice vector $\mathbf{a}_\alpha$, and for each Cartesian direction i

$$\sum_a \Lambda_{ai,\alpha j} = 0 \,. \tag{24}$$

Condition (24) always applies and can be exploited to generate the three rows of the Λ tensor corresponding to the three Cartesian displacements of an atom a^{TI} at almost no cost through the relation:

$$\Lambda_{a^{\mathrm{TI}}i,\alpha j} = -\sum_{b \neq a^{\mathrm{TI}}} \Lambda_{bi,\alpha j} \,. \tag{25}$$

2.4.2 Atomic Equivalences (AE)

The atomic equivalences introduced in Section 2.3.1 can be exploited to reduce the number of elements of the internal-strain tensor Λ to be explicitly computed. Let us introduce the 3×3 block $\Lambda^{a_1\alpha}$ of the internal-strain tensor proper of a symmetry-irreducible atom a_1 and of a given fundamental direct lattice vector $\mathbf{a}_\alpha$. The elements of the internal-strain tensor corresponding to symmetry-equivalent atoms a_s can be obtained by means of the following transformation:

$$\hat{R}_s \Lambda^{a_1\alpha} \hat{R}_s^{-1} = \sum_\beta c^s_{\alpha\beta} \Lambda^{a_s\beta} \,, \tag{26}$$

where $\hat{R}_s$ is one of the left-coset representative operators introduced in Eq. (18) and the extension of Eq. (22) to internal-strain components has been exploited.

According to the AE symmetry, only those rows of Λ that correspond to symmetry-irreducible atoms (three rows per atom; one for each Cartesian direction) must be evaluated while the others can be easily generated at almost zero cost through Eq. (26). In Section 2.4.3, the exploitation of atomic invariances will be shown to lead to a further reduction of the number of rows per atom to be explicitly evaluated for symmetry-irreducible atoms.

2.4.3 Atomic Invariance (AI)

Analogously to what has been shown by Stanton for the interatomic force-constant matrix $\mathbf{H}$,[19] the number of rows of the internal-strain tensor to be explicitly evaluated for each symmetry-irreducible atom can be reduced from 3 to 1 or 2 depending on whether the atom lies on a three-fold (or higher-order) rotation axis or on an order two symmetry operator other than inversion and identity (two-fold rotation axis or symmetry plane). A necessary condition for the aforementioned atomic invariances to be effectively exploited is the existence of at least one symmetry operator $\hat{R}_q$ belonging to the site-symmetry sub-group $\mathscr{H}_{a_1}$, defined in Section 2.3.1, which allows for the mixing between 3 or 2 Cartesian directions, respectively.

Before discussing how the AI symmetry applies to Λ, it is worth defining how Cartesian unit vectors $\mathbf{x}$, $\mathbf{y}$ and $\mathbf{z}$ transform upon

application of a symmetry operator:

$$\hat{R}_q \mathbf{i} = \sum_k d_{ik}^q \mathbf{k} \quad \text{with} \quad \mathbf{i},\mathbf{k} = \mathbf{x},\mathbf{y},\mathbf{z}\,, \tag{27}$$

where the d_{ik}^q coefficients are reals.

Let $\Lambda^{a_1 i\alpha}$ be a vectorial block of the internal-strain tensor corresponding to the i-th Cartesian displacement of the symmetry-irreducible atom a_1 and to the $\mathbf{a}_\alpha$ fundamental lattice vector. By application of a symmetry operator $\hat{R}_q \in \mathscr{H}_{a_1}$, it transforms as:

$$\hat{R}_q \Lambda^{a_1 i\alpha} = \sum_\beta c_{\alpha\beta}^q \left(\sum_k d_{ik}^q \Lambda^{a_1 k\beta} \right)\,, \tag{28}$$

which can be exploited to obtain at almost zero cost 1 or 2 rows per symmetry-irreducible atom depending on the nature of the corresponding site-symmetry sub-group.

3 The Implementation

In this section we shall briefly present the implementation of a scheme for the quantum-mechanical calculation of the internal-strain tensors Λ and Γ, which fully exploits all the symmetry-features introduced in Section 2.4. This scheme has been implemented into a developmental version of the public CRYSTAL14 program,[21] which allows for all-electron Gaussian-type function basis sets and several approximations of the exchange-correlation functional of the DFT (local-density, generalized-gradient, global and range-separated hybrid) to be used.

3.1 Internal-strain Tensor

Algorithms for the analytical evaluation of energy gradients with respect to both Cartesian atomic coordinates $\mathbf{f}_a$ and Cartesian lattice vector components $\mathbf{g}_\alpha$ have been implemented into the CRYSTAL program for periodic systems of any dimensionality by Doll and collaborators.[30–33]

The elements of the internal-stain tensor Λ can thus be obtained as numerical derivatives of lattice or atomic gradients according to either of the two equalities in Eq. (17), respectively. As such, the second equality would be preferred as it would involve just 6 lattice deformations instead of $3N$ atomic displacements. However, given that the $3N$ atomic displacements have anyhow to be performed for the evaluation of the Hessian matrix $\mathbf{H}$ (which is required to get Γ), the first equality in Eq. (17) is used as it reduces the total number of calculations from $3N+6$ to $3N$.

Thus, by taking advantage of analytical cell gradients, the elements $\Lambda_{ai,\alpha j}$ of the force-response internal-strain tensor are here computed as finite differences of $\mathbf{g}_\alpha$ with respect to atomic Cartesian displacements, by means of a generalized "Pulay's force method" originally proposed for interatomic force constants.[34] Single- and double-sided finite difference formula have been implemented, according to which:

$$\Lambda_{ai,\alpha j} = \left[\left.\frac{\partial E}{\partial a_{\alpha j}}\right|_{\{u\}=0;u_{ai}=\overline{u}} - \left.\frac{\partial E}{\partial a_{\alpha j}}\right|_{\{u\}=0} \right] / \overline{u}\,; \tag{29}$$

$$\Lambda_{ai,\alpha j} = \left[\left.\frac{\partial E}{\partial a_{\alpha j}}\right|_{\{u\}=0;u_{ai}=\overline{u}} - \left.\frac{\partial E}{\partial a_{\alpha j}}\right|_{\{u\}=0;u_{ai}=-\overline{u}} \right] / 2\overline{u}\,,$$

where $\overline{u}$ is the amplitude of the applied atomic displacement, with a default value of 0.003 Å. Use of the latter formula is generally preferable as it allows for the cancellation of contaminating effects of cubic anharmonicity.

The structure of the implementation is as follows:

1. A full symmetry analysis of the system is performed: the $N_{\text{at}}^{\text{irr}}$ symmetry-irreducible atoms a_1 are determined as well as the corresponding n_{a1}^{star} equivalent atoms in the *star*.

2. For each irreducible atom a_1, the number of Cartesian rows of the Λ tensor to be explicitly computed as analytical gradient finite differences is determined from the symmetry-invariance properties of atom a_1, according to the criteria introduced in Section 2.4.3. Symmetry-irreducible rows are computed via Eq. (29) or its double-sided analogue.

3. Symmetry-reducible Cartesian rows of each symmetry-irreducible atom a_1 are generated at almost zero cost by application of selected symmetry operators $\hat{R}_q$ belonging to the site-symmetry sub-group of atom a_1 through Eq. (28).

4. Once the three rows proper of each symmetry-irreducible atom a_1 have been obtained, the blocks of the Λ tensor corresponding to its symmetry-equivalent atoms a_s are generated at almost zero cost by the application of symmetry operators $\hat{R}_s$ (the left-coset representatives introduced in Eq. (18)) through Eq. (26).

5. If for one atom a^{TI} there are no symmetry-equivalent atoms ($n_{a^{\text{TI}}}^{\text{star}} = 1$), the "translational invariance" symmetry introduced in Section 2.4.1 can be effectively exploited to further reduce the number of rows to be actually evaluated through Eq. (29). Indeed, the three rows of atom a^{TI} can be obtained with Eq. (25), provided all the other atoms of the system have already been treated.

For symmetry-irreducible rows of symmetry-irreducible atoms, when the elements of Λ are computed as cell gradient finite differences through Eq. (29), a fourth kind of symmetry is exploited: the "residual symmetry". When an atom is displaced by $\overline{u}$ along a given Cartesian direction, the point-symmetry of the system is reduced but may not be completely lost; this residual symmetry can be exploited in the solution of the self-consistent-field (SCF) step and in the calculation of analytical energy gradients.

When passing from the force-response Λ to the displacement-response Γ internal-strain tensor, the interatomic force-constant matrix $\mathbf{H}$ is required, whose symmetry features are already fully-exploited in its calculation as implemented into the CRYSTAL program.[20] Given that the actual atomic Cartesian displacements to be considered for the SCF and analytical gradient calculation are the same for both objects, the current implementation for the internal-strain tensor has been devised in such a way to simultaneously compute Λ and $\mathbf{H}$, nearly at the same computational cost as for the calculation of $\mathbf{H}$ alone. The evaluation of Γ can thus be performed straightforwardly at the end of the calculation through the matrix multiplication in Eq. (5).

Table 1 For each of the six symmetric crystalline systems, a representative crystal is chosen, whose main symmetry features are given in the table. The number of point-symmetry operators N_{sym}, the total number of atoms per primitive cell N_{at} and the number of symmetry-irreducible atoms per primitive cell $N_{\text{at}}^{\text{irr}}$ are reported. The last three rows of the table report the total number of rows $N_{\text{rows}}^{\text{tot}}$ of the internal-strain tensor Λ that should be computed if symmetry was not to be exploited, the number of rows $N_{\text{rows}}^{\text{AE}}$ to be computed by exploiting just the AE symmetry, and the number of rows $N_{\text{rows}}^{\text{AE+AI}}$ to be computed by exploiting both the AE and AI symmetries.

Crystal	Pyrope	Zinc Oxide	α-Quartz	Urea	α-Forsterite	Coesite
Formula	$Mg_3Al_2(SiO_4)_3$	ZnO	SiO_2	$CO(NH_2)_2$	Mg_2SiO_4	SiO_2
Lattice	Cubic	Hexagonal	Trigonal	Tetragonal	Orthorhombic	Monoclinic
Space Group	$Ia\bar{3}d$	$P6_3mc$	$P3_221$	$P\bar{4}2_1m$	$Pbnm$	$C2/c$
N_{sym}	48	12	6	8	8	4
N_{at}	80	4	9	16	28	24
$N_{\text{at}}^{\text{irr}}$	4	2	2	5	6	7
$N_{\text{rows}}^{\text{tot}}$	240	12	27	48	84	72
$N_{\text{rows}}^{\text{AE}}$	12	6	6	15	18	21
$N_{\text{rows}}^{\text{AE+AI}}$	8	4	4	10	18	21

3.2 Nuclear-relaxed Elastic and Piezoelectric Tensors

Once the internal-strain tensor Λ and the interatomic force-constant matrix **H** have been computed, the evaluation of the nuclear-relaxation contribution $C_{v\mu}^{\text{nuc}}$ to the elastic constants can be performed rather straightforwardly either by the pseudo-inversion of **H** through Eq. (8) or by the diagonalization of its mass-weighted counterpart $\tilde{\mathbf{H}}$ through Eq. (13). Both approaches have been implemented. In the CRYSTAL program, the electronic clamped-nuclei term of the fourth-rank elastic tensor is obtained from finite differences of analytical cell gradients at strained lattice configurations.[7,8]

The evaluation of the nuclear-relaxation term of the third-rank "proper" direct piezoelectric tensor requires a further quantity to be computed: the effective Born charge tensor $\mathbf{Z}^*$ of Eq. (11). In the current implementation, advantage is taken of a fully-analytical scheme for the calculation of such a quantity, which is based on the Coupled-Perturbed-Hartree-Fock/Kohn-Sham (CPHF/KS) technique,[35,36] at variance with the usual numerical procedure based on the Berry-phase approach.[1–3] Also for piezoelectric constants, two strategies have been implemented for the nuclear-relaxation term, following Eq. (10) or Eq. (14), depending on whether the interatomic force-constant matrix is pseudo-inverted or diagonalized. In the CRYSTAL program, the electronic clamped-nuclei term can be computed numerically though a Berry-phase approach,[4,37–39] or analytically with a recently-developed CPHF/KS-based scheme.[29]

For both the elastic and piezoelectric tensors, before the current implementation, nuclear-relaxation terms were taken into account by performing geometry-optimizations[40] of the internal atomic positions at strained lattice configurations,[5,41–45] which is a rather slowly-converging numerical procedure compared to the evaluation of the internal-strain tensor, as it requires particularly tight convergence criteria.[18] While the present paper aims at documenting both the computational and numerical advantages (in terms of reduced computing time and increased numerical accuracy) due to the full symmetry-exploitation in the construction of the internal-strain tensor, a detailed numerical comparison between internal-strain and geometry-optimization strategies will be addressed in a forthcoming paper.

4 Results and Discussion

The effect of a full exploitation of symmetry is generally two-fold: on the one hand, it significantly reduces the computational cost of a calculation in terms of required memory and computing time; on the other hand, it contributes to increasing the numerical precision of the computed quantities. In this section, we shall discuss both effects.

4.1 Computational Performance

We start by documenting the gain factor in terms of computing time that can be achieved in the quantum-mechanical evaluation of the internal-strain tensor of crystals by fully exploiting its symmetry features introduced in Section 2.4. To do so, and to document the generality of the current implementation as well, we shall consider six crystals belonging to the six crystalline systems that are characterized by a certain degree of point-symmetry (all but the triclinic one): the most abundant member of the silicate garnet family of rock-forming minerals, Pyrope, is here taken as representative of cubic lattices, it belongs to the $Ia\bar{3}d$ space group and it is characterized by 48 symmetry-operators in the corresponding point-symmetry group; Zinc oxide is considered as a hexagonal crystal, which belongs to the $P6_3mc$ space group with 12 point-symmetry operators; α-Quartz represents trigonal lattices as it belongs to the $P3_221$ space group with 6 point-symmetry operators; the molecular crystal of Urea has been chosen to represent tetragonal lattices, it belongs to the $P\bar{4}2_1m$ space group and it exhibits 8 point-symmetry operators; as a representative of the orthorhombic crystals, we consider one of the main constituents of the Earth upper mantle, α-Forsterite, which belongs to the $Pbnm$ space group with 8 point-symmetry operators; finally, for the monoclinic crystalline system, a different polymorph of silica with respect to α-Quartz is considered, Coesite, which belongs

to the C2/c space group with 4 point-symmetry operators.

Selected symmetry features of these six crystals are given in Table 1, where the effect of the exploitation of the three symmetries discussed in Section 2.4 on the reduction of the number of rows of the internal-strain Λ tensor to be explicitly computed as cell gradient finite differences over displaced atomic configurations through Eq. (29) is quantified. The number of point-symmetry operators $N_{\rm sym}$, the total number of atoms per primitive cell $N_{\rm at}$ and the number of symmetry-irreducible atoms per primitive cell $N_{\rm at}^{\rm irr}$ are reported. The last three rows of the table refer to the internal-strain tensor and report the total number of rows $N_{\rm rows}^{\rm tot} = 3 \times N_{\rm at}$ that should be computed without exploiting any symmetry feature, the number of rows $N_{\rm rows}^{\rm AE}$ to be computed by exploiting just the "atomic equivalence" symmetry discussed in Section 2.4.2, and the number of rows $N_{\rm rows}^{\rm AE+AI}$ to be computed by exploiting also the "atomic invariance" symmetry discussed in Section 2.4.3. For none of these six crystals, the exploitation of the "translational invariance" symmetry discussed in Section 2.4.1 would lead to an actual reduction of the number of rows to be explicitly computed with respect to the AE and AI symmetries.

The following considerations can be made: i) in all cases (including those crystalline systems, such as monoclinic and orthorhombic, characterized by a relatively low point-symmetry), the reduction of the number of rows of the internal-strain tensor to be explicitly computed with costly SCF and gradient calculations is rather significant; ii) for Pyrope (a system characterized by many atomic equivalences) the gain factor is as large as 30, is about 7 for α-Quartz and is about 5 even for the tetragonal and orthorhombic representatives; iii) For the four crystals belonging to the most highly symmetric crystalline systems (cubic, hexagonal, trigonal and tetragonal) both the "atomic equivalence" and the "atomic invariance" symmetries contribute to the reduction of the number of symmetry-irreducible rows, whereas for the two orthorhombic and monoclinic crystals the "atomic equivalence" symmetry brings the whole reduction.

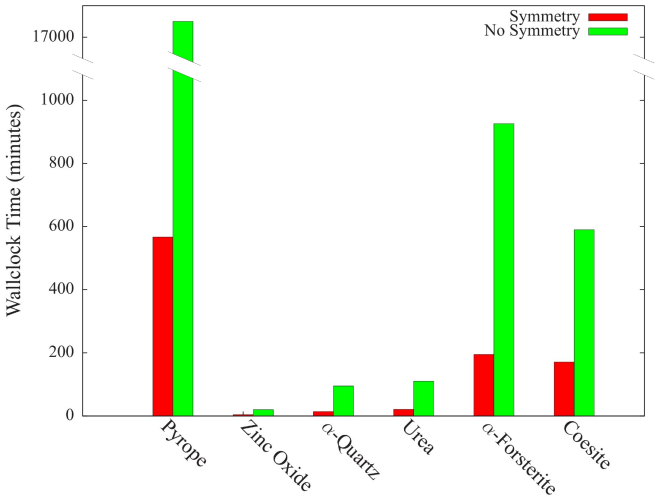

Fig. 1 (color online) Wallclock time (in minutes) for the calculation of the internal-strain tensors Λ and Γ by exploiting (red) or not (green) their symmetry features. Calculations are performed using the PBE exchange-correlation functional of the DFT and have been run in parallel over 16 processors on a Linux cluster of Intel-Xeon processors, working at 2.13 GHz.

Table 2 Nuclear contribution of non-null elastic constants C_{vw} (in GPa) and direct piezoelectric constants e_{kv} (in C/m^2) of Zinc Oxide as obtained by exploiting ("Sym") or not ("No Sym") symmetry in the evaluation of the internal strain tensor. Values are obtained both by using a single- and double-sided formula for cell gradient finite differences. The mean absolute deviation from zero $|\overline{\Delta}|$ of all of those constants that should vanish is also reported (in units of 10^{-4} GPa and 10^{-4} C/m^2 for elastic and piezoelectric constants).

	Single-sided		Double-sided	
	Sym	No Sym	Sym	No Sym
$C_{11}^{\rm nuc}$	-68.06	-66.97	-67.30	-66.95
$C_{22}^{\rm nuc}$	-67.58	-68.27	-67.30	-67.62
$C_{12}^{\rm nuc}$	29.00	28.41	28.47	28.78
$C_{13}^{\rm nuc}$	38.02	37.85	38.02	37.90
$C_{23}^{\rm nuc}$	38.02	37.96	38.02	38.04
$C_{33}^{\rm nuc}$	-74.47	-73.79	-74.46	-74.88
$C_{44}^{\rm nuc}$	-18.72	-18.80	-18.56	-18.79
$C_{55}^{\rm nuc}$	-18.72	-18.70	-18.56	-18.61
$\|\overline{\Delta}\|$	426	1154	3	43
$e_{15}^{\rm nuc}$	-0.811	-0.809	-0.810	-0.809
$e_{24}^{\rm nuc}$	-0.811	-0.809	-0.810	-0.809
$e_{33}^{\rm nuc}$	1.769	1.775	1.769	1.769
$e_{31}^{\rm nuc}$	-0.903	-0.911	-0.903	-0.908
$e_{32}^{\rm nuc}$	-0.903	-0.908	-0.903	-0.907
$\|\overline{\Delta}\|$	0	7	0	0

The actual gain due to the full exploitation of symmetry in terms of computing time for the calculation of the internal-strain tensors Λ and Γ for these six crystals is documented in Figure 1. In addition to the gain factor expected from the symmetry considerations (AE and AI) of Table 1, wallclock timings in Figure 1 (in minutes) also reflect the impact of the exploitation of the "residual symmetry" at displaced configurations, introduced in Section 3. All calculations have been performed with a developmental version of the CRYSTAL14 program,[21] by running in parallel mode over 16 Intel-Xeon processors working at 2.13 GHz, on a Linux cluster with Ethernet connection. The machine has 8 cores per node and 2 GB of memory per core. The PBE generalized-gradient exchange-correlation functional[46] is used in combination with all-electron basis sets of triple-zeta quality for all systems[47] but Pyrope.[48]

In the figure, the time required for computing the Λ and Γ internal-strain tensors without the exploitation of point-symmetry (in green) is compared to that required when point-symmetry is fully-exploited according to the implementation described in Section 3 (in red). For Coesite and α-Forsterite the observed gain factor almost coincides with the one that could be expected from Table 1, given that displaced atomic configurations are completely asymmetrical and thus no "residual symmetry" can be exploited. For the other four systems, where most of the displaced atomic configurations still exhibit a non-null point-symmetry, the "residual symmetry" is actually exploited and the observed gains are

Table 3 Nuclear contribution of non-null elastic constants C_{vw} (in GPa) and direct piezoelectric constants e_{kv} (in C/m^2) of α-Quartz as obtained by exploiting ("Sym") or not ("No Sym") symmetry in the evaluation of the internal strain tensor. Values are obtained both by using a single- and double-sided formula for cell gradient finite differences. The mean absolute deviation from zero $|\overline{\Delta}|$ of all of those constants that should vanish is also reported (in units of 10^{-4} GPa and 10^{-4} C/m^2 for elastic and piezoelectric constants).

	Single-sided		Double-sided	
	Sym	No Sym	Sym	No Sym
C_{11}^{nuc}	-240.15	-240.26	-240.23	-240.26
C_{22}^{nuc}	-240.35	-239.16	-240.23	-240.58
C_{12}^{nuc}	-70.85	-70.65	-70.60	-70.66
C_{13}^{nuc}	-115.29	-114.51	-115.47	-115.42
C_{23}^{nuc}	-115.29	-114.95	-115.47	-115.39
C_{33}^{nuc}	-176.03	-175.52	-176.58	-176.32
C_{44}^{nuc}	-113.46	-113.77	-113.10	-113.29
C_{55}^{nuc}	-113.46	-113.11	-113.10	-113.32
C_{14}^{nuc}	-31.42	-31.84	-30.90	-31.03
C_{24}^{nuc}	31.44	29.41	30.90	31.04
C_{56}^{nuc}	-31.40	-31.07	-30.90	-31.10
$\overline{\Delta}$	338	4790	34	249
e_{11}^{nuc}	0.336	0.334	0.335	0.335
e_{12}^{nuc}	-0.337	-0.335	-0.335	-0.335
e_{26}^{nuc}	-0.336	-0.335	-0.335	-0.335
e_{14}^{nuc}	-0.137	-0.139	-0.140	-0.140
e_{25}^{nuc}	0.137	0.141	0.140	0.140
$\overline{\Delta}$	2	3	0	0

always slightly more favorable than those of Table 1.

4.2 Nuclear-relaxed Elastic and Piezoelectric Constants

We shall now document the effect of symmetry-exploitation in the evaluation of the internal-strain tensors on the numerical accuracy of the computed nuclear-relaxation contribution of both elastic and piezoelectric constants. In order to do so, we restrict our attention to two piezoelectric crystals among those considered so far: Zinc Oxide and α-Quartz. The effect on computed values of using a single- or double-sided form of the cell gradient finite difference formula will also be explicitly documented.

Computed values of the nuclear relaxation term of elastic C_{vw} and piezoelectric e_{kv} constants of Zinc Oxide are reported in Table 2, as obtained by exploiting ("Sym") or not ("No Sym") symmetry in the evaluation of the internal strain tensor. By definition (see Eq. (7)), the 6×6 elastic tensor is symmetric, $C_{vw}\equiv C_{wv}$, so that we can restrict our attention to its 21 upper-triangular elements. Zinc Oxide has 8 non-null elastic constants: $C_{11}\equiv C_{22}$, C_{33}, $C_{44}\equiv C_{55}$, C_{12} and $C_{13}\equiv C_{23}$. The 3×6 piezoelectric tensor is characterized by 5 non-null constants: $e_{15}\equiv e_{24}$, e_{33} and $e_{31}\equiv e_{32}$. All these non-null constants are explicitly given in the table, along with an overall index $|\overline{\Delta}|$, which measures the mean absolute deviation from zero of the remaining vanishing constants.

From inspection of Table 2, the following considerations can be made: i) as expected, when symmetry is exploited, the equivalences among elastic ($C_{11}\equiv C_{22}$, $C_{44}\equiv C_{55}$ and $C_{13}\equiv C_{23}$) or piezoelectric ($e_{15}\equiv e_{24}$ and $e_{31}\equiv e_{32}$) constants are more accurately described compared to the case when symmetry is not exploited; ii) the full exploitation of point-symmetry provides a much cleaner description of the vanishing constants, reflecting an overall increased precision of computed values: for elastic constants, for instance, when symmetry is exploited, $|\overline{\Delta}|$ passes from 1154 to 426 or from 43 to 3 (in units of 10^{-4} GPa), depending on whether the single- or double-sided formula for finite differences is used; iii) passing from the single- to the double-sided formula for finite differences significantly increases the numerical precision of the computed elastic constants: when symmetry is exploited, the $C_{11}\equiv C_{22}$ equivalence is fully-recovered and $|\overline{\Delta}|$ decreases from 426 to 3; iv) values computed by exploiting symmetry are found to be more numerically stable while values obtained without a symmetry exploitation are changing more significantly when passing from a single- to a double-sided finite difference formula, for instance (see the e_{33} piezoelectric constant).

The computed nuclear-relaxation term of elastic and piezoelectric constants of α-Quartz is reported in Table 3, which has been given the same structure of the previously discussed Table 2. The α-Quartz crystal is characterized by 11 non-null elastic constants: $C_{11}\equiv C_{22}$, C_{33}, $C_{44}\equiv C_{55}$, C_{12}, $C_{13}\equiv C_{23}$, and $C_{14}\equiv C_{56}\equiv -C_{24}$. The piezoelectric tensor in this case has 5 non-null constants: $e_{14}\equiv -e_{25}$ and $e_{11}\equiv -e_{12}\equiv -e_{26}$. From inspection of Table 3, analogous considerations can be made to those just discussed for Zinc Oxide: i) when point-symmetry is fully-exploited and a double-sided formula for finite differences is used, the symmetry-equivalences among elastic and piezoelectric constants are nicely described, which is clearly not the case when symmetry is not exploited, even more so if a single-sided formula is adopted; ii) the overall numerical precision of the calculation is increased by the exploitation of symmetry, which is reflected in the lower value of $|\overline{\Delta}|$ with respect to the non-exploitation of symmetry: for elastic constants, it passes from 4790 to 338 and from 249 to 34 for single- and double-sided cases, respectively (in units of 10^{-4} GPa); iii) as expected and as already noticed above, use of a double-sided expression for the finite difference formula significantly increases the numerical precision of the computed elastic and piezoelectric constants.

5 Conclusions

The specific point-symmetry features of the internal-strain tensor of crystals have been illustrated and traced back to fundamental atomic equivalences and invariances. A computational scheme has been devised for their full-exploitation in the quantum-mechanical evaluation of nuclear-relaxation terms of strain-related elastic and piezoelectric properties of solids. The proposed computational method represents a generalization of Stanton's approach to point-symmetry exploitation in the interatomic force constant calculation according to "Pulay's force method".

The full symmetry exploitation in the construction of the internal-strain tensor has been documented to significantly reduce the cost of the calculation for crystals belonging to any non-asymmetric crystalline system (from cubic to monoclinic), and

to increase the numerical accuracy of computed nuclear-relaxed elastic and piezoelectric constants of two reference crystals: Zinc Oxide and α-Quartz. Work is currently in progress for a detailed comparison as regards both numerical accuracy and computational efficiency between an internal-strain tensor and a geometry optimization approach to nuclear-relaxed elastic and piezoelectric coefficients.

Acknowledgements Claudio Zicovich-Wilson and Michel Rérat are gratefully acknowledged for their fundamental support in my understanding of some subtle aspects of the point-symmetry and piezoelectricity of solids, respectively.

References

1 R. D. King-Smith and D. Vanderbilt, *Phys. Rev. B*, 1993, **47**, 1651.
2 D. Vanderbilt, *J. Phys. Chem. Solids*, 2000, **61**, 147.
3 R. Resta, *Rev. Mod. Phys.*, 1994, **66**, 899.
4 A. Erba, K. E. El-Kelany, M. Ferrero, I. Baraille and M. Rérat, *Phys. Rev. B*, 2013, **88**, 035102.
5 A. Mahmoud, A. Erba, K. E. El-Kelany, M. Rérat and R. Orlando, *Phys. Rev. B*, 2014, **89**, 045103.
6 B. B. Karki, L. Stixrude and R. M. Wentzcovitch, *Rev. Geophys.*, 2001, **39**, 507–534.
7 W. F. Perger, J. Criswell, B. Civalleri and R. Dovesi, *Comput. Phys. Commun.*, 2009, **180**, 1753–1759.
8 A. Erba, A. Mahmoud, R. Orlando and R. Dovesi, *Phys. Chem. Miner.*, 2014, **41**, 151–160.
9 D. Donadio, M. Bernasconi and F. Tassone, *Phys. Rev. B*, 2003, **68**, 134202.
10 F. Detraux and X. Gonze, *Phys. Rev. B*, 2001, **63**, 115118.
11 A. Erba and R. Dovesi, *Phys. Rev. B*, 2013, **88**, 045121.
12 A. Erba, M. T. Ruggiero, T. M. Korter and R. Dovesi, *J. Chem. Phys.*, 2015, **143**, 144504.
13 X. Wu, D. Vanderbilt and D. R. Hamann, *Phys. Rev. B*, 2005, **72**, 035105.
14 M. Veithen, X. Gonze and P. Ghosez, *Phys. Rev. B*, 2005, **71**, 125107.
15 J. F. Nye, *Physical properties of crystals*, Oxford University Press, Oxford, 1957.
16 G. Saghi-Szabo, R. E. Cohen and H. Krakauer, *Phys. Rev. Lett.*, 1998, **80**, 4321–4324.
17 A. Dal Corso, M. Posternak, R. Resta and A. Baldereschi, *Phys. Rev. B*, 1994, **50**, 10715–10721.
18 D. R. Hamann, X. Wu, K. M. Rabe and D. Vanderbilt, *Phys. Rev. B*, 2005, **71**, 035117.
19 J. F. Stanton, *Int. J. Quantum Chem.*, 1991, **39**, 19–29.
20 R. Dovesi, F. Pascale and C. Zicovich-Wilson, *Beyond Standard Quantum Chemistry: Applications from Gas to Condensed Phases*, Transworld Research Network, 2007, pp. 117–138.
21 R. Dovesi, R. Orlando, A. Erba, C. M. Zicovich-Wilson, B. Civalleri, S. Casassa, L. Maschio, M. Ferrabone, M. De La Pierre, Ph. D'Arco, Y. Noël, M. Causá, M. Rérat and B. Kirtman, *Int. J. Quantum Chem.*, 2014, **114**, 1287–1317.
22 R. Orlando, M. De La Pierre, C. M. Zicovich-Wilson, A. Erba and R. Dovesi, *J. Chem. Phys.*, 2014, **141**, 104108.
23 R. Dovesi, *Int. J. Quantum Chem.*, 1986, **29**, 1755–1774.
24 C. Zicovich-Wilson and R. Dovesi, *Int. J. Quantum Chem.*, 1998, **67**, 299–309.
25 C. Zicovich-Wilson and R. Dovesi, *Int. J. Quantum Chem.*, 1998, **67**, 311–320.
26 M. Springborg, V. Tevekeliyska and B. Kirtman, *Phys. Rev. B*, 2010, **82**, 165442.
27 M. Springborg and B. Kirtman, *Theor. Chem. Acc.*, 2011, **130**, 687–700.
28 I. Souza, J. Íñiguez and D. Vanderbilt, *Phys. Rev. Lett.*, 2002, **89**, 117602.
29 J. Baima, A. Erba, L. Maschio, C. Zicovich-Wilson, R. Dovesi and B. Kirtman, *Z. Phys. Chem.*, 2015, DOI: 10.1515/zpch–2015–0701.
30 K. Doll, *Comput. Phys. Commun.*, 2001, **137**, 74–88.
31 K. Doll, V. Saunders and N. Harrison, *Int. J. Quantum Chem.*, 2001, **82**, 1–13.
32 K. Doll, R. Dovesi and R. Orlando, *Theor. Chem. Acc.*, 2004, **112**, 394–402.
33 K. Doll, R. Dovesi and R. Orlando, *Theor. Chem. Acc.*, 2006, **115**, 354–360.
34 P. Pulay, *Mol. Phys.*, 1969, **17**, 197–204.
35 L. Maschio, B. Kirtman, R. Orlando and M. Rérat, *J. Chem. Phys.*, 2012, **137**, 204113.
36 L. Maschio, B. Kirtman, M. Rérat, R. Orlando and R. Dovesi, *J. Chem. Phys.*, 2013, **139**, 167101.
37 Y. Noël, M. Llunell, R. Orlando, Ph. D'Arco and R. Dovesi, *Phys. Rev. B*, 2002, **66**, 214107.
38 M. Catti, Y. Noël and R. Dovesi, *J. Phys. Chem. Solids*, 2003, **64**, 2183.
39 A. Erba, M. Ferrabone, J. Baima, R. Orlando, M. Rérat and R. Dovesi, *J. Chem. Phys.*, 2013, **138**, 054906.
40 B. Civalleri, Ph. D'Arco, R. Orlando, V. R. Saunders and R. Dovesi, *Chem. Phys. Lett.*, 2001, **348**, 131–138.
41 K. E. El-Kelany, A. Erba, P. Carbonnière and M. Rérat, *J. Phys.: Cond. Matter*, 2014, **26**, 205401.
42 K. E. El-Kelany, P. Carbonnière, A. Erba and M. Rérat, *J. Phys. Chem. C*, 2015, **119**, 8966–8973.
43 K. E. El-Kelany, P. Carbonnière, A. Erba, J.-M. Sotiropoulos and M. Rérat, *J. Phys. Chem. C*, 2016, **120**, 7795–7803.
44 J. Baima, A. Erba, R. Orlando, M. Rérat and R. Dovesi, *J. Phys. Chem. C*, 2013, **117**, 12864–12872.
45 V. Lacivita, A. Erba, Y. Noël, R. Orlando, Ph. D'Arco and R. Dovesi, *J. Chem. Phys.*, 2013, **138**, 214706.
46 J. P. Perdew, K. Burke and M. Ernzerhof, *Phys. Rev. Lett.*, 1996, **77**, 3865.
47 M. F. Peintinger, D. V. Oliveira and T. Bredow, *J. Comput. Chem.*, 2013, **34**, 451.
48 S. Casassa, A. Erba, J. Baima and R. Orlando, *J. Comput. Chem.*, 2015, **36**, 1940–1946.